Proceedings of the Estonian Academy of Sciences,
2015, **64**, 3S, 379–388
doi: 10.3176/proc.2015.3S.08
Available online at www.eap.ee/proceedings

NONLINEAR WAVES

Analysis of ship wake transformation in the coastal zone using time–frequency methods

Tomas Torsvik[a*], Heiko Herrmann[a,b], Ira Didenkulova[a,c**], and Artem Rodin[a,c]

[a] Institute of Cybernetics at Tallinn University of Technology, Akadeemia tee 21, 12618 Tallinn, Estonia
[b] Institute of Physics, Technische Universität Chemnitz, 09107 Chemnitz, Germany
[c] Nizhny Novgorod State Technical University n.a. R. E. Alekseev, Minin Str. 24, 603950 Nizhny Novgorod, Russia

Received 19 December 2014, accepted 30 June 2015, available online 28 August 2015

Abstract. Ship wake transformation in the coastal zone is analysed based on field measurements of wave conditions at two measurement sites located about 20 m and 100 m from the shore. Analysis of single wake events recorded at both sites is carried out by transforming the time series of the wave amplitude into the time–frequency domain, using both a short-time Fourier transform and a wavelet transform. Analysis reveals that signature features of individual wake components can be tracked as the wake approaches the shore, but the wave amplitude and associated wave energy is transformed differently for different wake components. The wake energy is reduced as the waves propagate through the surf zone, which can be attributed mainly to wave breaking of the leading wave system and a significant reduction of the divergent wave system. However, the energy of transverse waves is stable or increasing, indicating that these waves undergo a non-breaking shoaling process.

Key words: wave transformation, ship wake, wave energy, Fourier transform, wavelet transform.

1. INTRODUCTION

Waves in the coastal zone are transformed and amplified due to effects of wave shoaling, refraction, diffraction and wave breaking. This is a challenge with respect to coastal engineering and marine safety, where it is often important to take into account the impact of waves at the coast based on offshore wave conditions. One important category is waves generated by ships, in particular large, high-speed vessels, which may contribute significantly to the total wave impact at the coast [1].

Ship wakes are transient wave events that often involve a combination of several linear and nonlinear wave components [2], and their impact on the coast is often highly variable due to wave interaction with bottom topography [3]. According to the classical Kelvin wake theory [4], waves generated by vessels in deep water will be confined within a wedge-shaped region that in deep water has a half-angle (Kelvin angle) of 19.5°. However, the amplitude of individual wave components in the wake depends on the specific hull configuration, and hence wake characteristics may vary significantly for different ships [5,6]. Furthermore, recent studies have shown that the distribution of wave energy within the wake region can also be altered when ships are moving at high speed [7,8], specifically for length Froude numbers $F_{\mathrm{L}} = U/\sqrt{gL_{\mathrm{s}}} \gtrsim 0.5$, where U and L_{s} are the ship speed and length, respectively, and g is the gravitational acceleration. In shallow water the wave making resistance working against the forward propulsion of the ship will also depend on the local water depth d, as expressed by the depth-based Froude number $F_d = U/\sqrt{gd}$. The shallow water effect is particularly strong at $F_d > 0.6$ [9], when unsteady wave components can be generated [10,11].

Given the number of factors influencing ship wakes listed above, it is difficult to accurately predict the wake impact at a particular stretch of the coastline even if parameters related to ship route, ship dimensions, and ship speed are known. Likewise, it is difficult to

* Corresponding author, tomas.torsvik@ioc.ee
** Present address: Marine Systems Institute, Tallinn University of Technology, Akadeemia tee 15A, 12618 Tallinn, Estonia.

identify the source of individual wake components given a measurement record of a wake event at the coast. Traditional wave spectrum analysis does not provide a suitable framework for the identification of wake structures, due to the transient and spatially localized nature of ship wakes. However, these wave structures are naturally described in the time–frequency space by the use of local-transform methods such as short-time Fourier transforms or wavelet transforms. Recent studies [12,13] have made use of the short-time Fourier transform to produce spectrogram representations of wake events, which provide information about the energy content of individual wake components.

In this paper we apply the time–frequency representation to study the transformation of wake waves in the surf zone. It is well known that wave energy is dissipated in the surf zone due to wave breaking and reflection as waves interact with bottom topography. However, only a few studies have been made on the transformation of ship wakes in shallow water [3,14–16], and these studies did not provide information about the transformation of wave energy. In [16] the authors looked at the change in statistics of ship-induced waves within one wake during wave propagation and runup on the coast. Using the time–frequency representation, it is our aim not only to quantify the change in wave energy, but also to clarify how individual wake components are transformed in the surf zone. In the present study we have also included analysis based on wavelet transforms, aiming to obtain a representation that provides a clear separation between ship wake and wind wave components in the measurement data.

2. MEASUREMENT PROGRAM AND ANALYSIS

Ferry traffic between Tallinn and Helsinki is a source of potentially damaging wakes due to the relatively high speed (∼25 knots) of large ferries operating near the coast when arriving to and departing from Tallinn harbour. Tallinn Bay is an area in the north-eastern Baltic Sea, of about 10 km × 20 km in size, which is open to the Gulf of Finland in the north and partly in the west, with the city of Tallinn located at the south end of the bay. The coastline shape and the location of the islands of Naissaar and Aegna offer protection from wind waves from most directions, with the roughest seas produced during north-northwesterly storms. Ship wakes have been the subject of extensive studies in the Tallinn Bay area (Fig. 1), with field experiments carried out at two sites, Aegna Island in 2008 ([1,17]) and Pikakari beach in 2009 ([18,19]). In these experiments wave conditions were measured outside the surf zone, and beach profiles were conducted regularly to determine the impact of wake events. The experiments demonstrated that even a single wake event could have a profound impact with respect to coastal morphology [1]. However, the experiments did not provide information about the wave transformation within the surf zone.

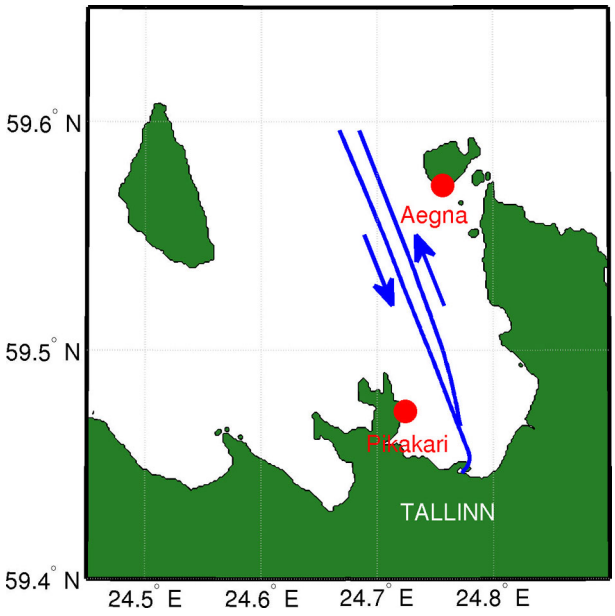

Fig. 1. Ferry fairways and field experiment sites in Tallinn Bay.

A field experiment was conducted in 2013 at Aegna Island, at the same location as the 2008 experiment. This time the waves were measured at two locations (Fig. 2), at approximately 100 m from the shore (Offshore Tripod Location, hereafter TPL-1) and at about 20 m from the shore (Onshore Tripod Location, hereafter TPL-2). TPL-1 (N59°34.276′, E24°45.287′) was located at a mean water depth of 2.7 m, and TPL-2 (N59°34.293′, E24°45.375′) was located at a mean water depth of 1.2 m. Steel tripod structures were used as mounting points for measurement instruments. The tripods were of similar design as used in the previous experiments [17]. The height above seabed of the tripod at TPL-2 was about 4 m, whereas an extension of 1 m brought the height of the tripod at TPL-1 to about 5 m. A LOG_aLevel® echosounder was mounted on top of each of the tripods (Fig. 2b), which provided a point measurement of the water level at the tripod site.

The study concentrated on analysis of wake from conventional ferries in the Tallinn Bay area, in particular the ferries *Star* and *Superstar* (described in [17]), which are known to be responsible for some of the largest wave loads on the coast [19]. Although these ferries are capable of speeds up to ∼ 25 knots, they normally run at reduced speeds in the shallowest coastal areas, hence the depth Froude number F_d is well below the critical level for these ships.

The largest wake events at Aegna were generated by ferries approaching from the south, and these waves would approach the measurement site from the south or southwest. Because TPL-1 was located about 90 m west-southwest of TPL-2, the waves approached the measurement site at an angle with respect to the line between the tripod locations. Hence the echosounders did not measure the same segment of the wake waves as they approached Aegna. However, the distance between

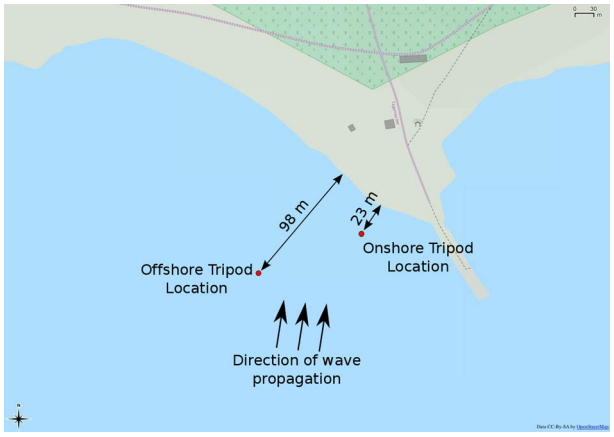

(a) 2013 Aegna experiment: Map of measurement locations

(b) A LOG_aLevel echosounder mounted on top of a tripod

(c) Offshore measurement locations seen from Aegna

(d) A ship wake

Fig. 2. Wave measurements at Aegna, 2013.

the tripod locations was smaller than the ship length, hence the wave generation parameters can be assumed to be identical. Furthermore, the wake waves are long crested, with minor variations along the crest. It is therefore assumed that the waves measured at TPL-1 are also representative of the offshore conditions south of TPL-2. In most cases wave breaking would occur between TPL-1 and TPL-2, resulting in significant wave transformation between the measurement points.

Wave measurements were made with a sampling frequency of 5 Hz. The echosounder at TPL-1 started recording on 27 June 2013. As the tripod at TPL-2 was deployed later, the echosounder at that location started recording on 29 June 2013. Due to technical issues with the echosounder at TPL-1, the only time when both echosounders were recording continuously was from 1 July 2013 to 2 July 2013. The wake events we consider in this paper are therefore confined within this time period.

Spectrogram analysis of wake events recorded by the LOG_aLevel instruments was performed in a similar manner as by Didenkulova et al. [12]. The records were first de-meaned and filtered by subtracting a 2 min running mean over the record to remove long-period oscillations. Analysis was performed in MATLAB®, using the spectrogram function from the Signal Processing Toolbox, with Hemming windows of 3 min and a 170 s window overlap. The Power Spectral Density (PSD) was plotted with a logarithmic colour scale.

Wavelet analysis of the same data was performed using GNU R [20] with the *wavethresh* toolbox by Nason et al. [21,22]. To remove the average, the data are first differentiated and the wavelet analysis performed on the differentiated data. Among the many available wavelets, the discontinuous wavelet transform with Daubechies wavelets was chosen, and the analysis was performed with depth 10.

3. RESULTS

3.1. Spectrogram analysis

Figure 3 shows spectrogram representations of three wake events within the time period 1–2 July 2013. All wake events correspond to ferries passing Aegna on a northward route. The first event (Fig. 3a,b) corresponds to the passing of the ferry *Star* in conditions where the contribution from wind-generated waves was relatively low. The general structure of this wake event was similar to records made for the *Star* in 2008 at the same location [12]. A large-amplitude wake packet is measured at

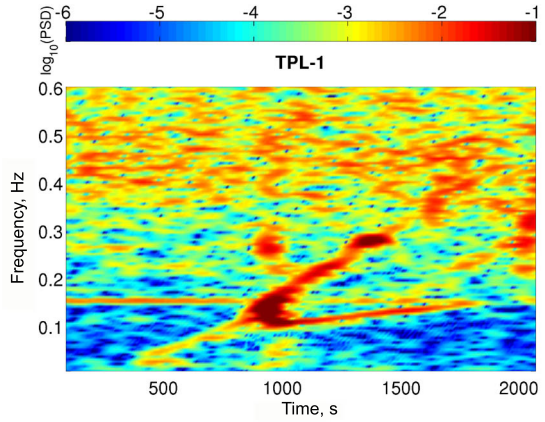

(a) TLP-1: 1 July 2013, 10:30, *Star*

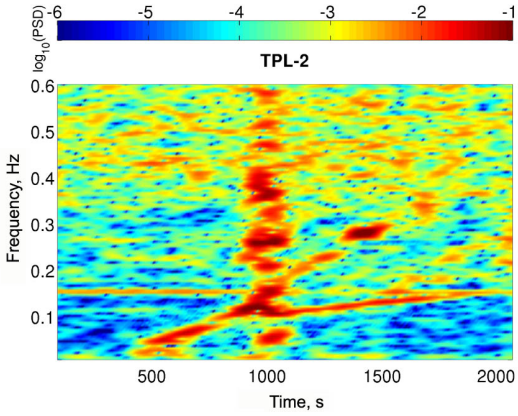

(b) TLP-2: 1 July 2013, 10:30, *Star*

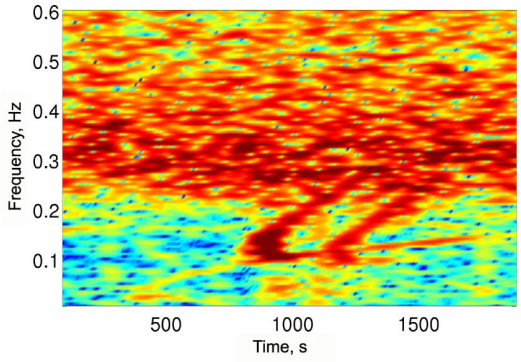

(c) TLP-1: 1 July 2013, 16:30, *Star*

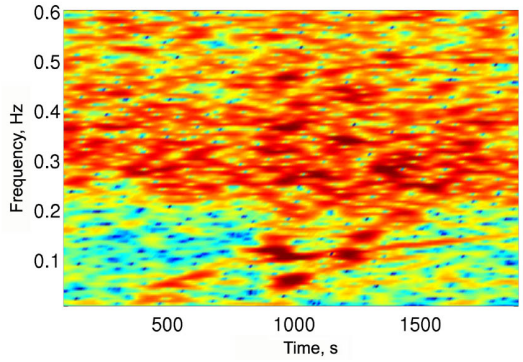

(d) TLP-2: 1 July 2013, 16:30, *Star*

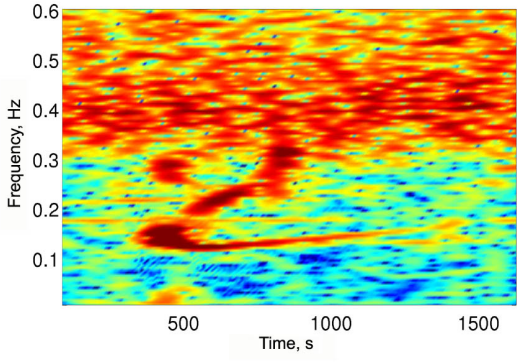

(e) TLP-1: 2 July 2013, 07:30, *Superstar*

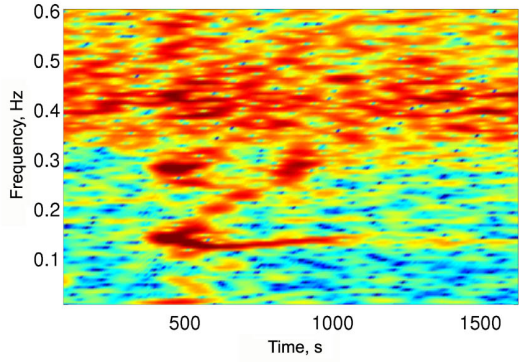

(f) TLP-2: 2 July 2013, 07:30, *Superstar*

Fig. 3. Wake events recorded at TLP-1 (left-hand column) and TLP-2 (right-hand column) on 1–2 July 2013. The date and time for each figure panel represent the starting time of the record.

about 1000 s, corresponding to waves near the edge of the wake wedge (the leading wave packet), which appears in the spectrogram as a vertical line. The low-frequency signal measured prior to this time corresponds to precursor waves, which are a specific feature for high-speed vessels in shallow water [9,10]. After 1000 s the wake structure splits into two clearly defined branches: a low-frequency (∼0.1–0.15 Hz) branch corresponding to transversal wake waves and a high-frequency 'chirp' signal corresponding to divergent wake waves [23]. In addition to contamination from wind-generated waves, seen as noise in the high-frequency part of the spectrum, there is a monochromatic wave with a frequency of about 0.15 Hz that persists throughout the record, which is probably due to an earlier wake event.

The second event (Fig. 3c,d) corresponds to the ferry *Star*, arriving at about 900 s, and another wake from an unknown ship arriving at 1200 s. In addition to the overlap of wake events, the wakes are partly masked by strong wind waves, appearing as random noise for wave frequencies larger than about 0.2 Hz. Hence this event is not suitable for analysis of wave transformation in the surf zone. However, it is interesting to compare this event with the previous one (Fig. 3a,b) as it is apparent that the wake structure, at least the low-frequency part that is visible in both cases, has clear similarities. This indicates that a ship will produce a wake event with similar structure at a single location if it repeatedly follows a similar track, which is usually the case for ferries following a regular schedule and route [23].

The third event (Fig. 3e,f) corresponds to the ferry *Superstar*, arriving at about 400 s. The wake event has a similar structure as the two *Star* wake events, except that there is no sign of a precursor wave. This indicates that the depth Froude number F_d was below the range required to generate unsteady wave components when passing the measurement site, and compared to the *Star* wakes, that either the ship speed was slower or that the route followed by the ship was in deeper water. Since the navigation corridors within Tallinn Bay are fairly narrow, about 800 m wide in the southern part, it is most probable that the speed of the *Superstar* was slower than of the *Star* in this case. The high-frequency components of the *Superstar* wake are masked by wind waves.

The transverse wave component for the single wake events is clearly visible and persists for over 15 min. In the double wake event (Fig. 3c,d) this effect is masked by the overlapping wave structures, hence it is not possible to determine the persistence of any one of them. It is also visible for all three events that the vertical structure corresponding to the leading wave packet becomes more prominent at the TPL-2 location.

Figure 4 shows how the wake event from the *Star* (1 July 10:30) is transformed in the surf zone. The top panel shows the original spectrograms at the TPL-1 and TPL-2 locations, whereas the bottom panels show the

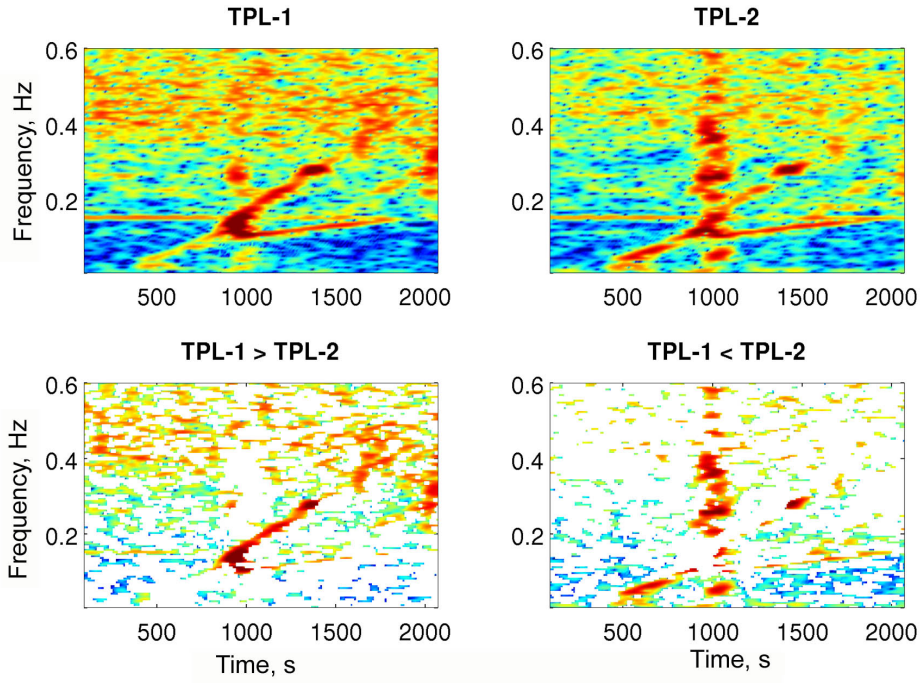

Fig. 4. Wake event generated by the *Star*, 1 July 2013, 10:30, recorded at TLP-1 (top left) and TLP-2 (top right). Bottom panels show regions of the spectrogram where TPL-1 has larger intensity than TPL-2 (bottom left), and where TPL-2 has larger intensity than TPL-1 (bottom right).

parts of the spectrogram where the PSD values are larger at TPL-1 than at TPL-2 (left-hand side), and vice versa (right-hand side panel). This is a rather crude way to compare the data at the two sites, but it illustrates some important points of the wave transformation in the surf zone. The most prominent feature is that the spectrum corresponding to the leading edge wave has a much wider spectrum at TPL-2 than at TPL-1. This is consistent with the nonlinear wave propagation and shoaling, which results in a deformation of the initial wave front to a steep one, and eventually leads to plunging wave breaking. This process was often observed at the coast during the experiment. The transverse wake component is not dominating at either site whereas the divergent wake component is more dominating at TPL-1 than at TPL-2, indicating that the divergent waves are strongly dissipative in the surf zone. However, the precursor wave is more dominant at TPL-2 than at TPL-1. This can be explained by shoaling effects, which lead to an increase in the potential energy of non-breaking waves when they are moving towards a shallower area. It is also possible that the long waves approaching from the south-west could partly be reflected from the pier and contribute to a wave focusing at TPL-2 (Fig. 2).

3.2. Results from wavelet analysis

Figure 5 shows wavelet representations of a wake event on 1 July 2013, corresponding to the passing of the ferry

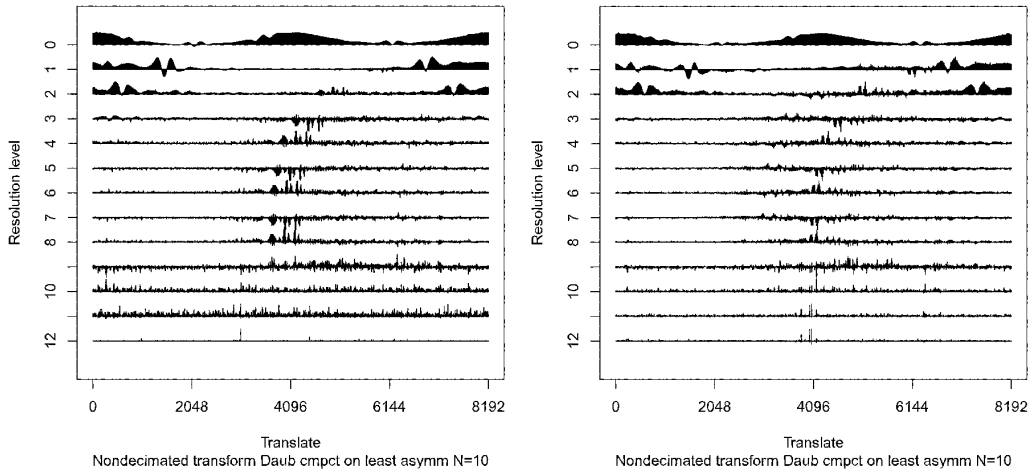

(a) TLP-1: 1 July 2013, 10:33.20, *Star*

(b) TLP-2: 1 July 2013, 10:33.20, *Star*

(c) |TLP-1| > |TLP-2|

(d) |TLP-2| > |TLP-1|

Fig. 5. Wavelet analysis of the wake events generated by the *Star*, 1 July 2013, 10:30, recorded at TLP-1 (a) and TLP-2 (b). Bottom panels show regions where the wavelet amplitude was larger for TPL-1 than for TPL-2 (c), and where the wavelet amplitude is larger for TPL-2 than for TPL-1 (d).

Star. This is the same wake event as shown in Fig. 4. Wavelet analysis requires the length of the data to be a power of two, therefore the data presented in Fig. 5a,b are cropped at the beginning and end (compared to Fig. 3a,b), so the wake event is centred in the data. The bottom panels of Fig. 5 show a rough analysis of the deformation of the wake when approaching the coast; Fig. 5c displays the wavelet coefficients where the absolute value at TLP-1 was larger than that at TLP-2 and Fig. 5d shows the opposite case, that is where the absolute value at TLP-2 was larger than that at TLP-1.

The wavelet representation in Fig. 5 is to some extent more difficult to interpret than the corresponding spectrogram representation (Fig. 4). For instance, the two branches corresponding to divergent and transverse waves are easily identified in the spectrogram, but can not be clearly distinguished from the background noise in the wavelet analysis. However, the wavelet analysis shows an interesting group structure present at several resolution levels, corresponding to the arrival of the leading wave system. This structure appears almost simultaneously at resolution levels 6–8, and with a gradual delay at lower resolution levels. The cause of this group structure and the reason for the delayed response at low resolution levels are not clear. However, this example illustrates that there may be structures hidden in the wake signal that are not represented by the short-time Fourier transform representation, in particular within the high-frequency range where wavelets can obtain a better resolution than is possible with short-time Fourier transforms.

3.3. Wake energy

In order to understand the impact of waves at the coast, it is necessary to quantify the energy that is being transmitted to the coast through the wave action. The potential energy associated with water displacement due to wave propagation can be calculated directly from the wave measurements

$$E = \rho g \int_{T_0}^{T_1} \eta^2 \, dt \,, \quad T_1 = T_0 + T_w \,, \tag{1}$$

where ρ is the density of water, η is the vertical free surface displacement, T_0 is the start time of the measurement, and T_w is the duration of the time window. The total wave energy includes the contributions both from wind- and ship-generated waves, and it does not provide information about the energy associated with individual wake components. As an alternative, Torsvik et al. [23] suggested that wave energy be calculated by integrating the power spectral density

$$E = \rho g \int_{T_0}^{T_1} \int_{-\infty}^{\infty} \mathrm{PSD}(\tau, f) \, df d\tau \,, \tag{2}$$

which is equivalent to Eq. (1) when integrating over the entire time window and frequency space, but can also be used to calculate wake energy associated with individual wake components.

An example outlining the procedure for the calculation of wake energy is illustrated in Fig. 6. The total wave energy is calculated for the time enclosed within the stippled black lines, marking the start and end times of the wake event. The first step of the procedure is to identify a representative background noise level $W(f)$, which is determined from the PSD field enclosed within the red stippled lines. A smooth function for the background noise level is constructed by averaging in time and applying a low-pass filter. Thereafter the parts of the PSD field corresponding to different wake components are identified, as illustrated by rectangles enclosed by white stippled lines in Fig. 6a. These component regions contain contributions both from the ship wake- and wind-generated waves. After removing the contribution that is defined by the representative background noise level

$$\mathrm{PSD}_{comp}(\tau, f) = \max\{\mathrm{PSD}(\tau, f) - W(f), 0\} \,,$$

we obtain a spectrogram decomposition (Fig. 1b) of the ship wake. The energy related to each wave component can now be calculated separately, and the total wake energy is the sum of the energy for each component. A similar analysis was previously carried out in [23] for ship wake measurements in the Tallinn Bay area.

Table 1 shows the potential energy for two wake events, measured at TPL-1 and TPL-2, and the relative contribution of different wake components as percentage of the total. The wake from the *Star* (1 July, 10:30) probably provided more reliable results than the wake from the *Superstar* (2 July, 07:30), as the former was recorded at a time when there were less small-scale local variations associated with wind-generated waves. As could be expected, the wave energy was reduced as waves propagated through the surf zone. For the *Star* wake, about 90% of the wave energy was conserved from TPL-1 to TPL-2. The largest contribution in each case was due to the leading waves. It is remarkable that the relative contribution of the leading waves increased slightly from TPL-1 to TPL-2, despite the strong wave transformation for these waves over the surf zone.

The largest reduction of wave energy was due to the divergent waves, whereas the energy associated with the precursor waves actually increased (from 0.4×10^3 J·s/m^2 to 2.7×10^3 J·s/m^2). A slight increase in the potential energy was also found for the transverse waves (from 2.1×10^3 J·s/m^2 to 2.7×10^3 J·s/m^2). The wake from the *Superstar* shows a similar reduction in divergent waves, whereas the contribution from the transverse waves was conserved from TPL-1 to TPL-2 (at about 3.9×10^3 J·s/m^2).

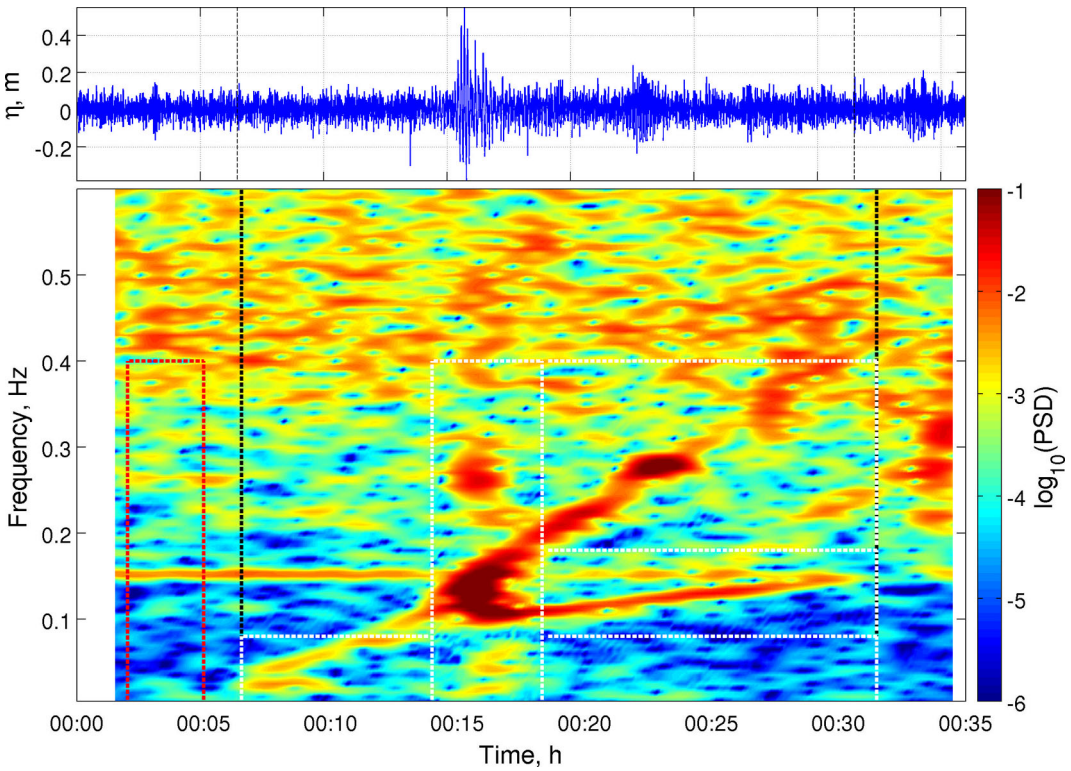

(a) Original spectrogram

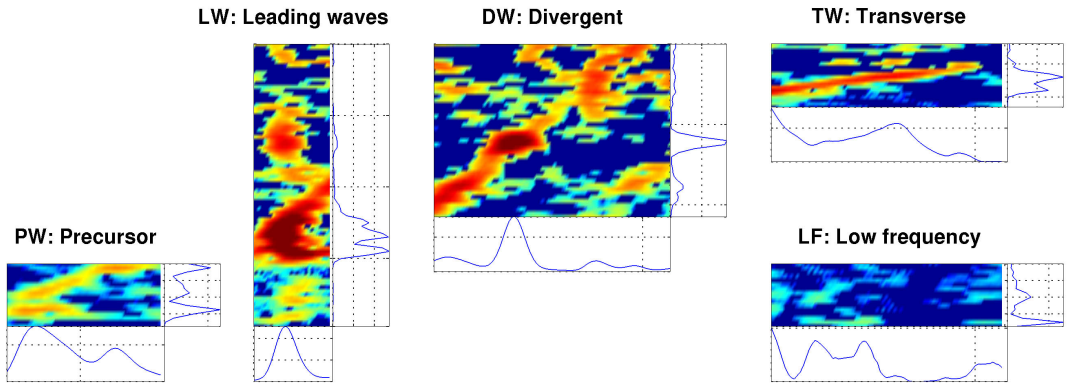

(b) Wake decomposition

Fig. 6. Wake energy. *Star*, 1 July 2013, 10:30, 100 m. The wave energy is calculated for the time enclosed within the stippled black lines. The background noise level is calculated from the PSD within the rectangle enclosed by red stippled lines. Rectangles enclosed by stippled white lines show the partitioning of the PSD into individual wake components. Panel (b) shows the decomposition where line plots along the *x*-axis and *y*-axis show the time- and frequency-integrated profiles, respectively.

In the surf zone it is expected that the potential energy for non-breaking waves will increase due to shoaling. For our measurements this can be estimated as

$$\Delta E \approx \sqrt{\frac{d_{\mathrm{TPL}-1}}{d_{\mathrm{TPL}-2}}} = \sqrt{\frac{2.7\,\mathrm{m}}{1.2\,\mathrm{m}}} = 1.5\,,$$

where $d_{\mathrm{TPL\text{-}1}}$ and $d_{\mathrm{TPL\text{-}2}}$ are water depths at the TPL-1 and TPL-2 locations, respectively. Hence, for non-breaking waves we can expect a 50% increase in the potential energy. The increase in the potential energy for the precursor waves in the *Star* wake can clearly not be explained by shoaling. It is therefore likely that either the bottom topography and coastline configuration contribute to the focus wave energy at TPL-2 or shield TPL-1 from the impact of the precursor waves. The increase in the potential energy for the transverse waves is well within the range as prescribed by the shoaling effect.

Table 1. Energy of wake events measured at TPL-1 and TPL-2. Energy of individual wake components is presented as percentage of the total wake energy. LW: leading waves; DW: divergent waves; TW: transverse waves; PW: precursor waves; LF: low-frequency trailing waves

Location	Total energy, $J \cdot s/m^2$	LW, %	Dw, %	Tw, %	PW, %	LF, %
		Star, 1 July 2013, 10:30				
TPL-1	4.26×10^4	66.7	27.2	5.1	1.0	0.1
TPL-2	3.91×10^4	67.2	18.8	6.8	6.9	0.2
		Superstar, 2 July 2013, 07:30				
TPL-1	6.86×10^4	64.1	30.0	5.7	0.1	0.1
TPL-2	4.15×10^4	70.1	19.7	9.5	0.1	0.5

The reduction in the potential energy for the divergent waves between TPL-1 and TPL-2 can probably be attributed to a combination of spilling wave breaking and wave reflection. A signature feature for plunging wave breaking, the transfer of wave energy to different frequencies, is clearly visible for the leading waves but not for the divergent waves. Whereas the plunging breaker results from a steep wave front, the spilling breaker is only present locally at the front end of the wave crest, causing a reduction in the wave height without significantly influencing the wave period. The expected signature feature of a spilling breaker is therefore a gradual increase in the high-frequency noise, but this can not be detected in the spectrograms due to the presence of noise from wind-generated waves. The reason why the wave reflection could be larger for divergent waves than for transverse waves is that waves with short periods are more sensitive than long waves to local variations in the bottom topography. The bottom topography in the study area was characterized by a combination of gravel and sparsely placed boulders. While the transverse waves could easily bypass the boulders, divergent waves were more likely to be strongly transformed by them.

4. DISCUSSION AND CONCLUSIONS

This study has demonstrated how time–frequency methods can be applied to analyse the transformation of ship wakes in the coastal zone. Although results have been obtained only for a few wake events, it has been clearly demonstrated that individual wake events preserve recognizable features throughout the surf zone. We are therefore in a position to investigate how the individual wake components are transformed while passing through the surf zone.

The most obvious change occurs in the leading wave train, the large amplitude wave packet associated with the leading edge of the wake wedge. During the transit through the surf zone, these waves transfer energy to both higher and lower frequencies, which is consistent with common features of the wave shoaling and breaking process. Although the potential energy of the leading waves was reduced over the surf zone, their relative contribution to the total potential energy slightly increased.

After the passing of the leading waves, the wake is dominated by relatively high-frequency divergent waves and to a less extent lower-frequency transverse waves. The potential energy of the divergent waves is strongly reduced during the transition through the surf zone, whereas it is increased for the transverse waves. This result indicates that the lower-frequency transverse waves can undergo a non-breaking shoaling process, whereas the higher-frequency divergent waves are transformed due to a combination of spilling breaking and wave reflection. This feature of the ship wake resembles what can happen in a sea when breaking wind waves are interacting with an underlying swell, and suggests that wake waves may be used to model this particular situation.

It has been observed on a number of occasions that ship wakes can have a profound effect on the coastal morphology, with even a single wake being capable of altering the beach profile [1]. The movement of sediments due to wave-induced currents is a highly complex process, where in addition to wave conditions, it is necessary to take into account sediment grain size and the friction acting between sediment particles. Under normal conditions the coast is usually in a semi-stable condition with a balanced sediment budget between deep and shallow water, except during storms, which disrupt the equilibrium [1,19]. Coasts that are exposed to frequent ship traffic can be impacted by short bursts of extreme waves at regular intervals, creating a highly dynamic morphological condition. The insight into the wake structure provided by the time–frequency methods used in this study can be of great value in determining if any single component of the wake is responsible for sediment disturbance, or if the effect is a result of a combination of components.

ACKNOWLEDGEMENTS

This research was supported by the European Union through the European Regional Development Fund, in particular through funding for the 'Centre for Nonlinear Studies' as an Estonian national centre of excellence, with additional support provided from institutional financing by the Estonian Ministry of

Education and Research (grant IUT-33-3). The assistance of the Tiger University Program of the Estonian Information Technology Foundation (VisPar system, EITSA grants 10-03-00-24, 12-03-00-11, and 13030009) is acknowledged. The work was also supported by grant MK-1146.2014.5, a grant from RFBR (15-35-20563), and by Russian State Contract No. 2014/133. T. Torsvik received support from the European Union through the Mobilitas grant MTT63. This article is dedicated to the memory of our dear colleague Dr Ewald Quak, who sadly passed away on 29 April 2015.

REFERENCES

1. Soomere, T., Parnell, K., and Didenkulova, I. Implications of fast ferry wakes for semi-sheltered beaches: a case study at Aegna Island, Baltic Sea. *J. Coastal Res.*, 2009, **SI 56**, 128–132.
2. Soomere, T. Nonlinear components of ship wake waves. *Appl. Mech. Rev.*, 2007, **60**(1–6), 120–138.
3. Torsvik, T., Didenkulova, I., Soomere, T., and Parnell, K. E. Variability in spatial patterns of long nonlinear waves from fast ferries in Tallinn Bay. *Nonlinear Proc. Geoph.*, 2009, **16**, 351–363.
4. Newman, J. N. *Marine Hydrodynamics*. The MIT Press, 1977.
5. Stumbo, S., Fox, K., Dvorak, F., and Elliot, L. The prediction, measurement, and analysis of wake wash from marine vessels. *Marine Technology*, 1999, **36**(4), 248–260.
6. Varyani, K. S. Full scale study of the wash of high speed craft. *Ocean Eng.*, 2006, **33**, 705–722.
7. Darmon, A., Benzaquen, M., and Raphael, E. Kelvin wake pattern at large Froude numbers. *J. Fluid Mech.*, 2014, **738**, R3.
8. Noblesse, F., He, J., Zhu, Y., Hong, L., Zhang, C., Zhu, R., and Yang, C. Why can ship wakes appear narrower than Kelvin's angle? *Eur. J. Mech. B-Fluid.*, 2014, **46**, 164–171.
9. Lee, S., Yates, G. Y., and Wu, T. Y. Experiments and analysis of upstream-advancing solitary waves generated by moving disturbances. *J. Fluid Mech.*, 1989, **199**, 569–593.
10. Akylas, T. R. On the excitation of long nonlinear water waves by a moving pressure distribution. *J. Fluid Mech.*, 1984, **141**, 455–466.
11. Mei, C. C. Radiation of solitons by slender bodies advancing in a shallow channel. *J. Fluid Mech.*, 1986, **162**, 53–67.
12. Didenkulova, I., Sheremet, A., Torsvik, T., and Soomere, T. Characteristic properties of different vessel wake signals. *J. Coastal Res.*, 2013, **SI 65**, 213–218. ICS 2013 Proceedings, Plymouth, UK.
13. Sheremet, A., Gravois, U., and Tian, M. Boat-wake statistics at Jensen Beach, Florida. *J. Waterw. Port Coast. Ocean Eng.*, 2013, **139**(4), 286–294.
14. Belibassakis, K. A. A coupled-mode technique for the transformation of ship-generated waves over variable bathymetry regions. *Appl. Ocean Res.*, 2003, **25**, 321–336.
15. Didenkulova, I., Parnell, K., Soomere, T., Pelinovsky, E., and Kurennoy, D. Shoaling and runup of long waves induced by high-speed ferries in Tallinn Bay. *J. Coastal Res.*, 2009, **SI 56**, 491–495.
16. Didenkulova, I. and Rodin, A. A typical wave wake from high-speed vessels: its group structure and run-up. *Nonlinear Proc. Geophys.*, 2013, **20**, 179–188.
17. Parnell, K., Delpeche, N., Didenkulova, I., Dolphin, T., Erm, A., Kask, A., et al. Far-field vessel wakes in Tallinn Bay. *Estonian J. Eng.*, 2008, **14**, 273–302.
18. Kurennoy, D., Parnell, K. E., and Soomere, T. Fast-ferry generated waves in south-west Tallinn Bay. *J. Coastal Res.*, 2011, **SI 64**, 165–169.
19. Didenkulova, I. and Soomere, T. Formation of two-section cross-shore profile under joint influence of random short waves and groups of long waves. *Marine Geol.*, 2011, **289**(1–4), 29–33.
20. R Development Core Team. *R: A Language and Environment for Statistical Computing*. R Foundation for Statistical Computing, Vienna, Austria, 2010.
21. Nason, G. P. *Wavelet Methods in Statistics with R*. Springer, 2008.
22. Nason, G. *wavethresh: Wavelets Statistics and Transforms*. R package version 4.6.6. http://CRAN.R-project.org/package=wavethresh (accessed 15.12.2014).
23. Torsvik, T., Soomere, T., Didenkulova, I., and Sheremet, A. Identification of ship wake structures by a time-frequency method. *J. Fluid Mech.*, 2015, **765**, 229–251.

Kiirlaevalainete üksikute komponentide omaduste muutumine rannikuvööndis

Tomas Torsvik, Heiko Herrmann, Ira Didenkulova ja Artem Rodin

Kiirlaevalainete ümberkujunemist rannikuvööndis on analüüsitud 20 ja 100 m kaugusel rannajoonest tehtud mõõtmiste alusel. Veepinna kuju ja lainete amplituudide aegjadad üksikutes laevalainete rühmades on teisendatud aja-sageduse koordinaadistiku salvestuste lühikestele lõikudele rakendatud Fourier' teisenduse abil ning lainikute meetodiga. On näidatud, et laevalainete süsteemi üksikute komponentide signatuur on selgelt jälgitav ühest mõõtepunktist teise, kuid erinevaid komponente esindavate lainete amplituudid ja potentsiaalne energia muutuvad erinevas rütmis. Suur osa laevalainete süsteemi koguenergia kahanemisest murdlainete vööndis tuleneb süsteemi esimeste, kõrgeimate ja pikimate lainete osalisest murdumisest ning põiklainete kõrguse kahanemisest. Seevastu pikilained levivad praktiliselt rannikuni ilma murdumata ja nende energia püsib peaaegu muutumatuna või isegi suureneb veidi.